Systematic study of subbarrier fusion in rare-earth nuclei

A. B. Balantekin and J. R. Bennett
Physics Department, University of Wisconsin, Madison, Wisconsin 53706
and Institute for Nuclear Theory, University of Washington, Seattle, Washington 98195

S. Kuyucak
Department of Theoretical Physics, Research School of Physical Sciences,
Australian National University, Canberra, Australian Capital Territory 0200, Australia and
Institute for Nuclear Theory, University of Washington, Seattle, Washington 98195
(Received 25 May 1993)

The recent accurate measurements of fusion cross sections at subbarrier energies have enabled extraction of barrier distributions which could provide a novel test for collective models. We carry out a systematic study of subbarrier fusion in rare-earth nuclei using a scheme which incorporates the interacting boson model for nuclear structure effects. The existing data on vibrational and rotational nuclei are fitted with a consistent set of parameters which are then used to predict the fusion cross sections and distribution of barriers in transitional nuclei. Contrary to vibrational and rotational nuclei where the cross sections increase smoothly with increasing deformation or mass number, transitional nuclei exhibit sharp changes in the barrier distribution due to shape-phase transitions. An accurate measurement of fusion cross sections for Pt and Os nuclei could thus provide a sensitive test for competing models in this region.

PACS number(s): 25.70.Jj, 24.10.Eq, 21.60.Fw, 27.70.+q

I. INTRODUCTION

Enhancement of subbarrier fusion cross sections in medium and heavy mass nuclei due to coupling of internal degrees of freedom to the relative motion is a well-established phenomenon (see Refs. [1,2] for a review). Until recently it was thought that the fusion cross sections are smooth functions of energy and could be reproduced by any model which included some coupling mechanism. This view that fusion cross sections are featureless and do not provide a good test for models has been challenged in a series of high-precision experiments at the Australian National University (ANU). The ANU group, following the suggestion of Rowley *et al.* [3], carried out accurate measurements of fusion cross sections for the reactions ^{16}O + ^{144,148,154}Sm and ^{16}O + ^{186}W, and determined the distribution of barriers directly from the fusion data [4–6]. Barrier distributions are rather sensitive to the details of nuclear structure and hence can provide a good test for various subbarrier fusion models.

In a series of papers [7–10], we have developed a model for subbarrier fusion which incorporates the interacting boson model (IBM) [11] to describe the nuclear structure effects. In a first attempt [8], the path integral method [7] and the SU(3) limit of the IBM were used to describe the reaction ^{16}O + ^{154}Sm which showed the feasibility of the approach. In Ref. [9], the SU(3) limit was replaced with the $1/N$ expansion [12] of the wave functions which allowed more realistic calculations. These calculations employed the usual linear coupling approximation. Most recently, using a Green function technique [13], we were able to include couplings to all orders going beyond the linear coupling approximation [10]. The formalism, in its present form, describes the nuclear structure effects in subbarrier fusion accurately, with all the approximations justified.

The purpose of this paper is to present a systematic study of subbarrier fusion in rare-earth nuclei. In Sec. II we give a brief review of the formalism discussing some of the finer approximations that were not studied previously. In Sec. III we discuss the effects of couplings on fusion cross sections and barrier distributions for a variety of nuclear shapes, e.g., spherical, vibrational, rotational, and transitional. In Sec. IV, the available high-precision data are fitted using a global nuclear potential and coupling parameters that are consistent with the experimental $E2$ and $E4$ transition strengths. Based on the systematic study in Sec. III we expect the transitional Os and Pt nuclei to show the most dramatic changes in cross sections and barrier distributions. Since there are no data available in this region, we have extended our calculations to Os and Pt nuclei to point out these effects and stimulate further experiments.

II. SUBBARRIER FUSION IN THE IBM

The application of the IBM to subbarrier fusion is discussed at length in Refs. [8–10] to which we refer for details. In this section we briefly review the formalism mainly to motivate the parameters used in the calculations as well as some of the approximations that were not discussed in the previous work. The Hamiltonian for the fusing system can be written as

$$H = H_k + H_{\rm IBM}(\xi) + V(\mathbf{r}, \xi), \tag{1}$$

where $\mathbf{r}$ is the relative coordinate of the two nuclei and ξ represents the internal (bosonic) degrees of freedom of the target nucleus. H_k is the kinetic energy operator for the system and $H_{\rm IBM}$ is an appropriate IBM Hamiltonian for the target nucleus which we take to be

$$H_{\rm IBM} = \epsilon_d n_d + \kappa Q \cdot Q. \tag{2}$$

Here n_d is the number operator for d bosons and Q is the quadrupole operator

$$Q = [s^\dagger \tilde{d} + d^\dagger s]^{(2)} + \chi [d^\dagger \tilde{d}]^{(2)}. \tag{3}$$

The parameters ϵ_d, κ, and χ describing the boson interactions are determined within the IBM from fitting the low-lying spectrum and transitions of the nucleus being investigated. The operators $s^\dagger$ (s) and $d^\dagger$ (d) create (annihilate) bosons of angular momentum zero and two, respectively. In the IBM, these bosons represent correlated pairs of valence nucleons. The brackets denote angular momentum coupling of two boson operators. The interaction between the internal system and the motion of the nuclei, $V(\mathbf{r},\xi)$, consists of the Coulomb and nuclear parts which we take as [14]

$$V_{\rm Coul}(\mathbf{r},\xi) = \begin{cases} \frac{Z_1 Z_2 e^2}{r}\left(1 + \frac{3}{5}\frac{R_1^2}{r^2}\hat{O}\right) & (r > R_0)\ , \\ \frac{Z_1 Z_2 e^2}{r}\left(1 - \frac{(R_0-r)^4(r^2+4rR_0+30R_1R_2-5R_0^2)}{160R_1^3R_2^3} + \frac{3}{5}\frac{r^2}{R_1^2}\hat{O}\right) & (R' < r < R_0)\ , \\ \frac{Z_1 Z_2 e^2}{r}\left(\frac{3r}{2R_1} - \frac{3rR_2^2}{10R_1^3} - \frac{r^3}{2R_1^3} + \frac{3}{5}\frac{r^2}{R_1^2}\hat{O}\right) & (0 < r < R'), \end{cases} \tag{4}$$

and

$$V_{\rm nuc}(\mathbf{r},\xi) = -V_0\left(1 + \exp\frac{r - R_0 - R_1\hat{O}(\hat{\mathbf{r}},\xi)}{a}\right)^{-1}. \tag{5}$$

The subscripts 1 and 2 refer to the target and the projectile nuclei, $R_0 = R_1 + R_2$, and $R' = R_1 - R_2$. It is assumed that $R_2 < R_1$. $\hat{O}$ is a coupling operator between the internal coordinates and the relative motion which includes the quadrupole and hexadecapole interactions

$$\hat{O} = u_2 Q \cdot Y^{(2)}(\hat{\mathbf{r}}) + u_4 [d^\dagger \tilde{d}]^{(4)} \cdot Y^{(4)}(\hat{\mathbf{r}}), \tag{6}$$

where, following the consistent-quadrupole formalism (CQF) of Ref. [15], the same quadrupole operator of Eq. (3) is used as in the IBM Hamiltonian of Eq. (2). The u_k represents the strengths of the various multipole transitions in the target nucleus. Note that the matrix elements of the interaction (6) between eigenstates of the IBM Hamiltonian in Eq. (2) scale as N, the number of bosons. Therefore, in order to keep the average interaction energy constant, u_k must scale as $1/N$. Thus, we introduce the reduced strengths v_k as

$$u_k = v_k / \langle 2_1 || Q || 0_1 \rangle. \tag{7}$$

The quadrupole matrix element in Eq. (7) is given to order $1/N$ by [12]

$$\langle 2_1 || Q || 0_1 \rangle = (N+1)(2x_0x_2 + \bar{\chi}x_2^2) + \bar{\chi}/2, \tag{8}$$

where x_0 and x_2 are the mean fields for the s and d bosons, and $\bar{\chi} = -\sqrt{2/7}\chi$. The $1/N$ correction term in Eq. (8), i.e., the second term in $N(1+1/N)$, is important for a quick convergence of the results with a low boson number. In earlier work, this term was ignored leading to a slow convergence with N and hence requiring much longer computation time. To give an example, results for the fusion cross section which are converged to within 5–10% of the exact answer are obtained with $N = 4$ when Eq. (8) is used whereas $N \sim 10$ is needed when only the leading term is included. As each additional boson number roughly doubles the CPU time, this rather simple point makes a big difference in computation time (minutes vs hours), and is essential in a systematic study such as this. Ideally, the quadrupole and hexadecapole strengths in (6) should be scaled with their respective matrix elements, however such a scaling leads only to a renormalization of the value of the hexadecapole coupling v_4 and has been ignored for simplicity.

The nuclear potential as given in Eqs. (5) and (6) contains couplings to all orders in u_2 and u_4 of Eq. (6), i.e., we do not expand the exponential to only first order as has been done previously, but evaluate its matrix element directly using the Green function technique [10]. In contrast, the Coulomb potential (4) is truncated at the first order. This is not because of any calculational difficulty but because inclusion of the second-order terms in (4) led to no visible difference. A further approximation in the Coulomb potential is the use of r^{-2} for the hexadecapole term instead of r^{-4}, which is for calculational convenience. We have studied this approximation using the CCDEF code [16]. The use of r^{-2} led to a slight change in the results which could be compensated by using a slightly larger v_4 in the approximate calculations.

We calculate the total fusion cross section using the partial wave expansion in the barrier penetration picture

$$\sigma_{\rm fus}(E) = \frac{\pi\hbar^2}{2\mu E}\sum_{\ell=0}^{\infty}(2\ell+1)T_\ell(E), \tag{9}$$

where T_ℓ are the penetration probabilities for the different partial waves which can be evaluated numerically using a uniform WKB approximation , valid for energies both above and below the barrier [17]

$$T_\ell(E) = \sum_{\{n_{\nu k}\}} |\langle\{n_{\nu k}\}|0_1\rangle|^2 \left[1 + \exp\left(2\sqrt{\frac{2\mu}{\hbar^2}}\int_{r_1}^{r_2} dr[V(r,\langle\hat{O}_D\rangle) - E]^{\frac{1}{2}}\right)\right]^{-1}, \quad (10)$$

where r_1 and r_2 are the classical turning points of the motion, and $|\{n_{\nu k}\}\rangle$ refers to the number representation in the interaction basis which diagonalizes the operator $\hat{O}$ with the expectation value $\langle\hat{O}_D\rangle$. This result, derived in Ref. [10], is the familiar representation of the subbarrier fusion cross section as a weighted average of cross sections due to tunneling through a set of potential barriers determined by the eigenvalues of the coupling operator. As has been emphasized by many authors [18,19], the validity of this expression depends only on the usual adiabatic and rotating frame approximations which we have discussed previously [9]. Algebraic expressions for the overlaps and $\langle\hat{O}_D\rangle$ in (10) are given in Ref. [10].

III. NUCLEAR STRUCTURE SYSTEMATICS

Before proceeding with the fits to the data, we present a sytematic study of the nuclear structure effects for various shapes. This will be helpful not only for an intuitive understanding of the existing data but will also suggest new experiments in uncharted territories where interesting results could be expected. The parameters of the Woods-Saxon potential are determined from a global fit which will be discussed in the next section. To isolate individual effects, we consider a fictitious nucleus with the mean fields and bare potential for ^{170}Yb but with variable values of quadrupole and hexadecapole couplings in all the schematic calculations in this section.

One convenient way to highlight the effects of nuclear structure on subbarrier fusion is to look at the energy derivative of the s-wave transmission probability, since the spread in energy of this quantity represents the distribution of barriers [3]. Classically, the transmission probability is a step function which goes from one to zero at an energy equal to the height of the barrier. Tunneling effects smear the step function into a smoother function (for a parabolic barrier this smooth function is a Fermi function). Hence the energy derivative of the transmission probability is a narrow peak centered around the barrier energy. If several barriers are present due to channel couplings, the energy derivative of the transmission probability will become a series of peaks corresponding to the energies of the different barriers. The heights of the peaks give the relative weights which the different barriers contribute to the total transmission probability.

To connect this quantity to the experimentally measured fusion cross sections, we can approximate the ℓ dependence of the transmission probability at a given energy by simply shifting the energy [20]:

$$T_\ell \sim T_0\left[E - \frac{\ell(\ell+1)\hbar^2}{2\mu R^2(E)}\right], \quad (11)$$

where $\mu R^2(E)$ characterizes an effective moment of inertia. Experimentally $R(E)$ was found to be a slowly varying function of energy [21]. If many values of ℓ are important in the sum over partial-wave transmission probabilities in Eq. (9), we can approximate that sum with an integral over ℓ, and, using Eq. (11) obtain [20,22]

$$E\sigma(E) = \pi R^2(E)\int_{-\infty}^{E} dE' T_0(E'). \quad (12)$$

It was found that Eqs. (11) and (12) represent the experimental data for both the total fusion cross section and the average orbital angular momentum rather well [22,21]. Differentiating Eq. (12) twice one obtains the energy derivative of the transmission probability to be proportional to the quantity [3]

$$D(E) \sim \frac{d^2}{dE^2}[E\sigma(E)] + \mathcal{O}\left(\frac{dR}{dE}\right). \quad (13)$$

Since $R(E)$ is a slowly varying function of energy, the first term in Eq. (13) will be used to give the distribution of barriers.

Figure 1 shows the effect of quadrupole coupling on fusion cross section and barrier distribution as the nucleus changes from spherical ($v_2 = 0$, dotted line), to vibrational ($v_2 = 0.12$, dashed line), and to prolate rotational ($v_2 = 0.24$, solid line). The other parameters used in the

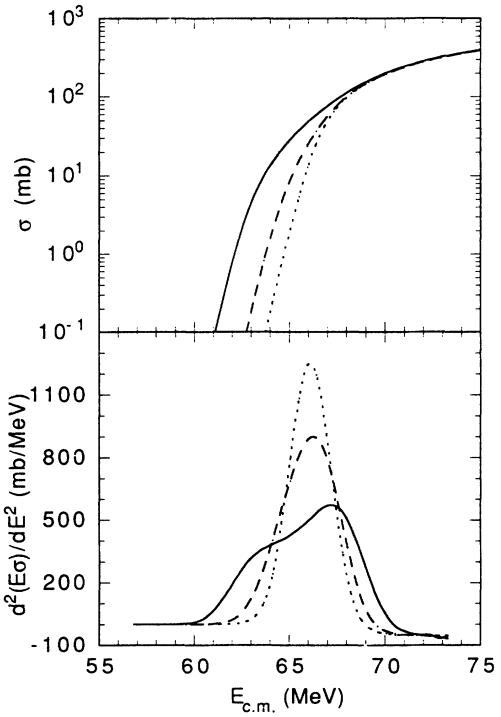

FIG. 1. The effect of quadrupole coupling on fusion cross section (top) and distribution of barriers (bottom) for various interaction strengths. The dotted, dashed, and solid lines are for $v_2 = 0, 0.12, 0.24$, corresponding to spherical, vibrational, and deformed nuclei, respectively.

TABLE I. Nuclear structure and interaction strength parameters used in the calculations for the rare-earth nuclei.

Nucleus	x_0	x_2	χ	v_2	v_4
^{144}Sm	0.95	0.31	-1.15	0.10	0.0
^{148}Sm	0.92	0.39	-1.15	0.18	0.0
^{154}Sm	0.74	0.67	-1.15	0.26	0.18
^{170}Yb	0.64	0.77	-0.66	-	-
^{186}W	0.68	0.73	-0.60	0.25	-0.05
^{192}Os	0.69	0.72	-0.20	0.19	-0.08
^{194}Pt	0.69	-0.72	0.15	0.17	-0.09

calculation are given in Table I. The asymmetric barrier distribution in the prolate case is the result of the axially symmetric deformation. In the geometrical model, the two peaks are associated with the fusion along the semimajor and semiminor axes which we will denote as the "prolate" and "oblate" peaks, respectively. In the case of the prolate peak, the nuclear potential extends out more compared to the spherical nuclei, and hence the barrier is shifted to a lower energy. For the oblate peak the opposite happens and the barrier is shifted to a higher energy. The barrier distribution follows from averaging over all orientations. Since there are two semiminor axes against one semimajor axis, the oblate peak clearly carries more weight and forms the maximum. With increasing deformation, the weight of the prolate peak is reduced, resulting in a more asymmetric barrier distribution favoring the oblate peak.

In deriving the eigenvalues of the coupling operator which appear in Eq. (10), one solves a quadratic equation similar to the eigenmode equation [23] encountered in the calculation of energy surfaces of individual nuclei in the IBM. The two roots, positive and negative, of the eigenmode equation correspond to the prolate and oblate minima in the energy surface. Similarly here, the positive and negative eigenvalues obtained in the interaction representation are associated with the prolate and oblate peaks in the barrier distribution. For a prolate nucleus, the root corresponding to the oblate peak is smaller (in absolute value) than the one corresponding to the prolate peak. The weights associated with these eigenvalues, given in Eq. (10), are larger for the oblate peak than for the prolate one. Hence in the distribution of barriers one finds a large peak (corresponding to the large weight) at an energy only slightly above the energy of the "bare" potential (corresponding to the small eigenvalue), and a smaller peak (corresponding to the smaller weight) at an energy well below the energy of the "bare" potential (corresponding to the large, negative eigenvalue). Also, for a prolate nucleus the parameter χ is negative. Increasing the value of $|\chi|$ leads to a more prolate-deformed nucleus which also results in a more asymmetric barrier distribution. Thus there is a one-to-one correspondence between the geometric model and the IBM descriptions of subbarrier fusion in deformed nuclei.

In Fig. 2 we show the effect of the hexadecapole force on a prolate nucleus. Increasing v_4 enhances the cross sections and favors the oblate peak in the barrier distributions as opposed to the prolate peak. This can be

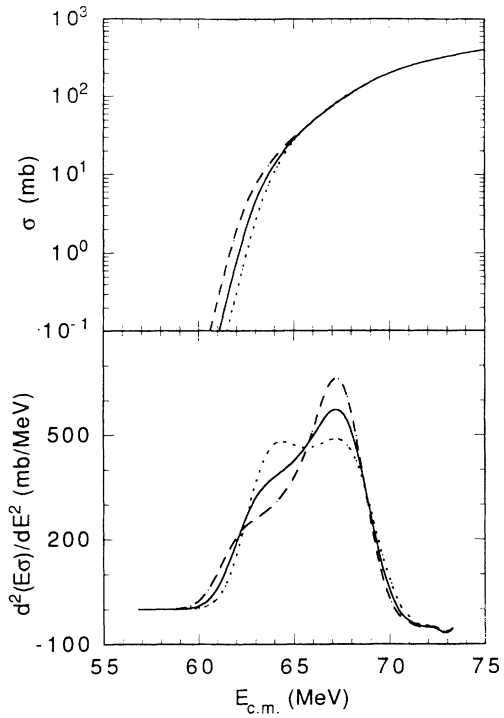

FIG. 2. Same as Fig. 1 but showing the effect of the hexadecapole coupling on a prolate target nucleus. The dotted, solid, and dashed lines denote $v_4 = -0.08, 0.0, +0.08$.

intuitively understood from the geometrical picture associated with the quadrupole and hexadecapole deformations. For a prolate shape, addition of a $\beta_4 > 0$ leads to a "top"-like shape which enhances the prolate character of the nucleus whereas addition of a $\beta_4 < 0$ leads to a "beer can" shape which is more oblatelike. Since the nuclear potential extends out more in a prolate shape the cross section is more enhanced in that case. In the barrier distribution figures this effect is noticeable by the appearance of more weight given to the very lowest barriers when $\beta_4 > 0$. Figure 3 shows the similar situation in an oblate nucleus. The weights of the prolate and oblate peaks are reversed but the effect of the hexadecapole force remains the same; increasing v_4 enhances the cross sections and favors the oblate peak in the barrier distribution. A different study [24] of the effects of hexadecapole moments in subbarrier fusion gave similar results.

In Fig. 4, the effect of the quadrupole coupling on prolate (dashed line), oblate (dotted line), and γ-unstable nuclei (solid line) is shown. The γ-unstable shape corresponds to an average of other shapes which is why its cross section is very close to the prolate one. Note however that this similarity has completely disappeared in the barrier distributions with the γ-unstable nucleus assuming a more symmetric shape. This figure also shows the power of the barrier distribution as an experimental tool where small differences in cross sections are converted to large effects which may be more easily identified. Finally, we show in Fig. 5 the barrier distributions in the three limits of the IBM, namely, the SU(5) (dot-

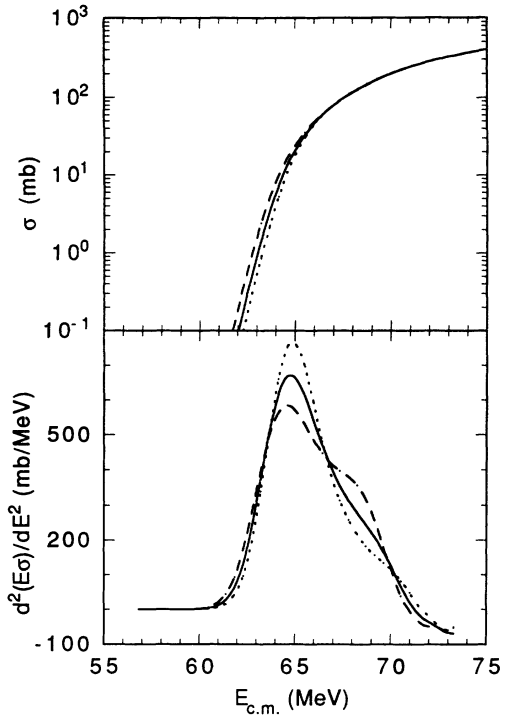

FIG. 3. Same as Fig. 2 but for an oblate target nucleus. The dotted, solid, and dashed lines denote $v_4 = -0.08, 0.0, +0.08$ as before.

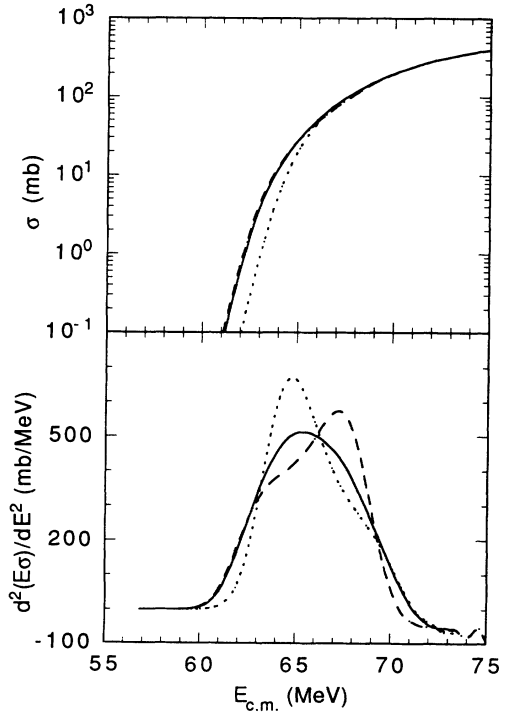

FIG. 4. The effect of quadrupole coupling in deformed nuclei with prolate (dashed line), oblate (dotted line), and γ-unstable (solid line) shapes. The hexadecapole coupling is set to zero.

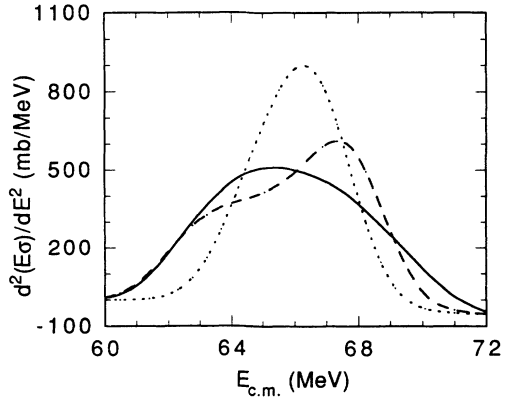

FIG. 5. Barrier distributions in the three limits of the IBM. The dotted, dashed and solid lines correspond to the SU(5), SU(3), and the O(6) dynamical symmetries.

ted line), SU(3) (dashed line), and O(6) (solid line) which represent the vibrational, rotational, and γ-unstable nuclei.

IV. APPLICATION TO RARE-EARTH NUCLEI

In this section we present the results of a global fit to the accurate fusion cross section and barrier distribution data measured by the ANU group in the rare-earth region. The nuclei encompass a wide range of quadrupole and hexadecapole deformations and correspondingly show a variety of behavior in the fusion data. In these calculations we have used a simple global parametrization of the Woods-Saxon potential, taking in all cases $R_2 = 2.62$ fm, $R_1 = 1.04A_1^{\frac{1}{3}}$ fm, $V_0 = 67.5(A_1/144)^{1/3}$ MeV, $a = 1.22$ fm. The mean fields x_0 and x_2 were determined from a given IBM Hamiltonian (which fits the low-lying spectroscopic data) by variational techniques [12]. The adjustable parameters were the quadrupole and hexadecapole interaction strengths, v_2 and v_4. All of these parameters are listed in Table I.

The results for ^{16}O on ^{144,148,154}Sm and ^{186}W are compared with the experimental data in Figs. 6–9. In all these figures the experimental barrier distribution points (shown in the lower panels) were deduced in Refs. [4–6] from the cross section data using a finite-difference approximation for the second derivative. In these references the energy step size used in the finite-difference formula was 2 MeV in the laboratory. Since the four lowest energy points are spread over an interval of less than 2 MeV, for these energies the barrier distributions were not deduced in Refs. [4–6]. Also note that the cross section data at the highest energies in Refs. [4–6] are not shown in our figures since we are concentrating on the subbarrier region. In general the calculations match both the cross section and the barrier distribution data quite well. The interaction strengths v_2 and v_4 which we found to best describe the data are consistent with the known $E2$ and $E4$ matrix elements for these nuclei. In particular, the v_2 values are very similar to the β_2 deformation parame-

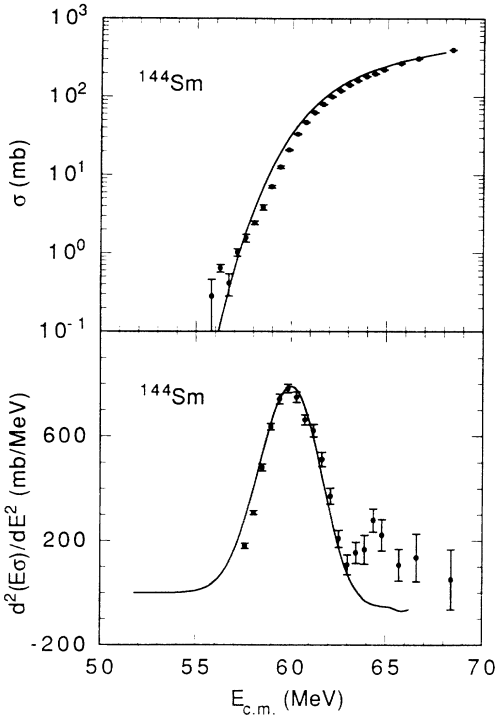

FIG. 6. Comparison of predicted fusion cross section and barrier distribution with the experimental data for the reaction $^{16}O + ^{144}Sm$. The coupling parameters are given in Table I. The ANU data shown in the figure are preliminary [6].

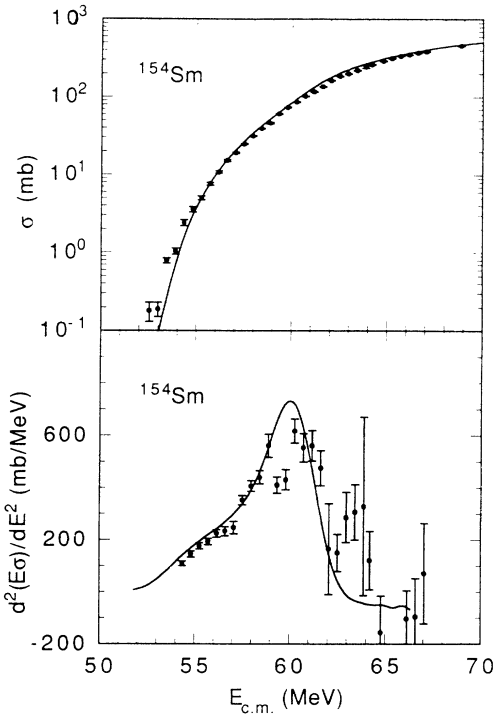

FIG. 8. Same as Fig. 6 but for ^{154}Sm. The data are from [4,5].

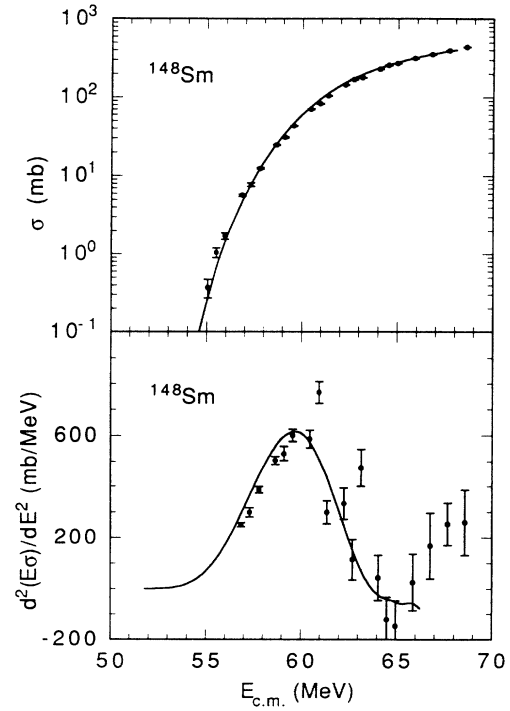

FIG. 7. Same as Fig. 6 but for ^{148}Sm. The data are from [6].

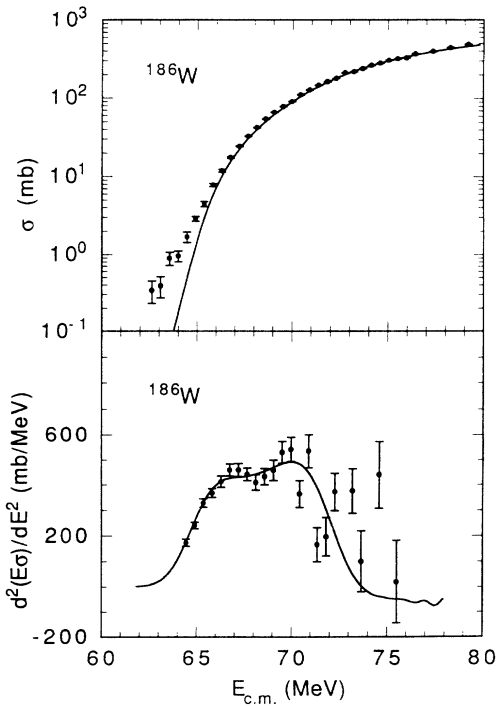

FIG. 9. Same as Fig. 6 but for ^{186}W. The data are from [6].

ters used for these nuclei. The v_4 values are a factor 2–3 larger than the β_4 values which is due to the fact that the hexadecapole operator used in the sd model is an effective one which underestimates the true strength. For example, the hexadecapole charge necessary to describe the $B(E4)$ values in the Sm isotopes is a factor of 3 larger in the sd model as compared to the sdg model [25].

The trends in the data are easily understood in the light of the nuclear structure systematics discussed in Sec. III. In particular, we note the large increase in quadrupole coupling strength in going from the spherical ^{144}Sm nucleus to the vibrational ^{148}Sm and rotational ^{154}Sm nuclei, and the corresponding increase in the fusion cross sections and widening of the barrier distributions. Also, in comparing ^{154}Sm with ^{186}W one should point out that although both nuclei are prolate, the sign of hexadecapole moment changes from positive for the former to negative for the latter. As was discussed in Sec. III, this has a large effect on the barrier distribution. For ^{154}Sm, the hexadecapole coupling enhances the prolateness to skew the barrier distribution even more, whereas for ^{186}W the two couplings interfere and hence the barrier distribution becomes more symmetric than for a pure prolate case.

Having demonstrated the ability of our model to describe well the available fusion data, we can now proceed with some confidence to consider other rare-earth nuclei for which subbarrier fusion has not been measured. The Os-Pt region would be interesting to study since these nuclei go through a shape transition from prolate to oblate as one increases the number of protons from 76 to 78. The resulting effect on the barrier distribution should be noticeable by the skewness toward higher energies for prolate nuclei and toward lower energies for oblate nuclei. To illustrate quantitatively the type of effect we expect, we show in Fig. 10 the calculated fusion cross sections and barrier distributions for the fusion reactions ^{16}O + ^{192}Os, ^{194}Pt. We used the same global parametrization of the nuclear potential and chose the interaction strengths to correspond to the measured $E2$ and $E4$ matrix elements for these nuclei [26]. The Pt cross section is much smaller than the Os one due mainly to the higher Coulomb barrier. However, in the barrier distribution one clearly sees the effect of the shape transition. The difference between the prolate and oblate distributions is partially masked by the smaller values of $|\chi|$ and the large negative hexadecapole moments which favor the oblate peak in both nuclei. Nevertheless, the prolate (first) peak is still prominent in ^{192}Os leading to a double hump structure whereas the second peak has almost disappeared in ^{194}Pt. Thus a precision measurement of fusion cross sections in these two nuclei should be able to distinguish between the barrier distributions relatively easily.

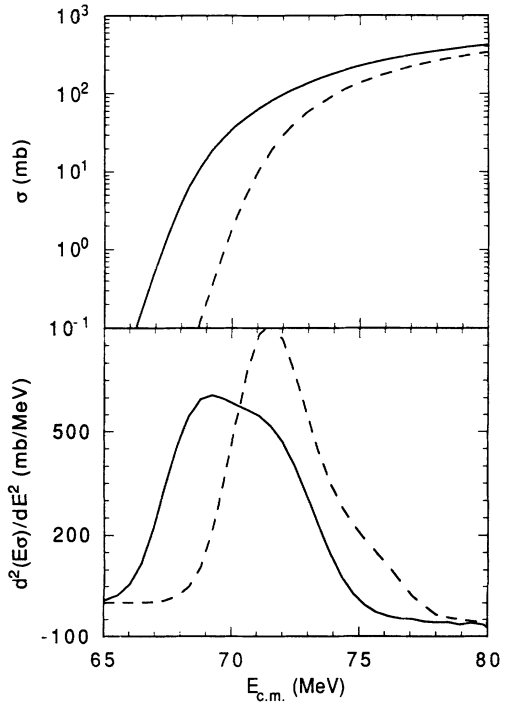

FIG. 10. Predicted fusion cross sections and barrrier distributions for the reactions ^{16}O + ^{192}Os (solid line) and ^{16}O + ^{194}Pt (dashed line).

V. SUMMARY AND CONCLUSIONS

We have performed a global analysis of subbarrier fusion data for rare-earth targets. Using the interacting boson model allows us to describe a variety of nuclear structure effects in these reactions. With the confidence gained from the model's successful description of the available data, we have calculated the fusion cross sections and barrier distributions for the reactions ^{16}O + ^{192}Os, ^{194}Pt. The prolate-oblate phase transition in this region should give rise to noticeable effects in the fusion barrier distribution, which we hope will stimulate further experimental efforts to study these reactions.

The Xe-Ba nuclei exhibit characteristics similar to the transitional Os-Pt region. These nuclei are not as well studied as the Os-Pt isotopes, and very basic information, such as whether they are prolate or oblate, is still missing. Subbarrier fusion could be an effective experimental tool in learning more about the Xe-Ba region and answer some interesting questions, e.g., whether they also undergo a shape-phase transition.

ACKNOWLEDGMENTS

This research was supported in part by the U.S. National Science Foundation Grant No. PHY-9314131, in part by the Australian Research Council, and in part by an exchange grant from the Department of Industry, Technology, and Commerce of Commonwealth of Australia. We thank J.R. Leigh for providing the data before publication and R. Vandenbosch for useful discussions and comments on an earlier version of this paper. We also thank the Institute for Nuclear Theory at the University of Washington for its hospitality and the Department of Energy for partial support during the course of this work.

[1] M. Beckerman, Rep. Prog. Phys. **51**, 1047 (1988).
[2] R. Vandenbosch, Annu. Rev. Nucl. Part. Sci. **42**, 447 (1992).
[3] N. Rowley, G.R. Satchler, and P.H. Stelson, Phys. Lett. B **254**, 25 (1991).
[4] J.X. Wei, J.R. Leigh, D.J. Hinde, J.O. Newton, R.C. Lemmon, S. Elfstrom, J.X. Chen, and N. Rowley, Phys. Rev. Lett. **67**, 3368 (1991).
[5] J.R. Leigh, N. Rowley, R.C. Lemmon, D.J. Hinde, J.O. Newton, J.X. Wei, J.C. Mein, C.R. Morton, S. Kuyucak, and A.T. Kruppe, Phys. Rev. C **47**, R437 (1993).
[6] R.C. Lemmon, J.R. Leigh, J.X. Wei, C.R. Morton, D.J. Hinde, J.O. Newton, J.C. Mein, M. Dasgupta, and N. Rowley, Phys. Lett. B **316**, 32 (1993); J.R. Leigh *et al.*, in Proceedings of the RIKEN Workshop on Heavy-Ion Reactions with Neutron-Rich Beams, Japan, 1993 (to be published).
[7] A.B. Balantekin and N. Takigawa, Ann. Phys. (N.Y.) **160**, 441 (1985).
[8] A.B. Balantekin, J.R. Bennett, and N. Takigawa, Phys. Rev. C **44**, 145 (1991).
[9] A.B. Balantekin, J.R. Bennett, A.J. DeWeerd, and S. Kuyucak, Phys. Rev. C **46**, 2019 (1992).
[10] A.B. Balantekin, J.R. Bennett, and S. Kuyucak, Phys. Rev. C **48**, 1269 (1993).
[11] F. Iachello and A. Arima, *The Interacting Boson Model* (Cambridge University Press, Cambridge, England, 1987).
[12] S. Kuyucak and I. Morrison, Ann. Phys. (N.Y.) **181**, 79 (1988).
[13] N. Takigawa, Y. Alhassid, and A.B. Balantekin, Phys. Rev. C **45**, 1850 (1992); A.B. Balantekin, J.R. Bennett, N. Takigawa, and Y. Alhassid, Jpn. J. Appl. Phys. Series **9**, 90 (1993).
[14] M.W. Kermode, M.M. Mustafa, and N. Rowley, J. Phys. G **16**, L299 (1990).
[15] R.F. Casten and D.D. Warner, Rev. Mod. Phys. **60**, 389 (1988).
[16] J. Fernandez Niello, C.H. Dasso, and S. Landowne, Comput. Phys. Commun. **54**, 409 (1989).
[17] D.M. Brink, *Semi-classical Methods for Nucleus-Nucleus Scattering* (Cambridge University Press, Cambridge, England, 1985).
[18] M.A. Nagarajan, A.B. Balantekin, and N. Takigawa, Phys. Rev. C **34**, 894 (1986).
[19] N. Rowley, Jpn. J. Appl. Phys. Series **9**, 218 (1993).
[20] A.B. Balantekin, S.E. Koonin, and J.W. Negele, Phys. Rev. C **28**, 1656 (1983).
[21] M. Dasgupta, A. Navin, Y.K. Agarwal, C.V.K. Baba, H.C. Jain, M.L. Jhingan, and A. Roy, Phys. Rev. Lett. **66**, 1414 (1991).
[22] A.B. Balantekin and P.E. Reimer, Phys. Rev. C **33**, 379 (1986).
[23] J.N. Ginocchio and M.W. Kirson, Nucl. Phys. **A350**, 31 (1980).
[24] J. Fernandez-Niello and C.H. Dasso, in *Proceedings of the Symposium on Heavy Ion Reactions Around the Coulomb Barrier, Legnaro, Italy*, edited by C. Signorini, S. Skorka, P. Spolaore, and A. Vitturi, Lecture Notes in Physics Vol. 317 (Springer, Berlin, 1988), p.56.
[25] S. Kuyucak and V-S. Lac, Phys. Rev. C **47**, 1815 (1993).
[26] V-S. Lac and S. Kuyucak, Nucl. Phys. **A539**, 418 (1992).